

# Improving the helium gas barrier properties of epoxy coatings through the incorporation of graphene nanoplatelets and the influence of preparation techniques

---

LJ van Rooyen<sup>\*a,b</sup>, J Karger-Kocsis<sup>b,c</sup>, LD Kock<sup>a</sup>

<sup>a</sup> Applied Chemistry, South African Nuclear Energy Corporation SOC Limited, P.O Box 582, Pretoria, 0001, South Africa

<sup>b</sup> Tshwane University of Technology (TUT), Faculty of Engineering and the Built Environment, P.O. Box 680, Pretoria, 0001, South Africa

<sup>c</sup> MTA-BME Research Group for Composite Science and Technology, Muegyetem rkp. 3, H-1111 Budapest, Hungary

**Abstract:** Graphene/epoxy nanocomposite coatings were formulated by applying different dispersion and preparation methods to determine whether the coatings might be a potential gas barrier material for irradiated graphite waste which is known to release radioactive gases like tritium ( $^3\text{H}_2$ ). Helium was used as a substitute gas for tritium and the gas permeability was measured with the use of a helium leak detector. The dispersion and fabrication techniques influenced the ability of the coatings to reduce the helium gas permeability. Characterisation of the graphene nanoplatelets and the composite morphology showed that the dispersion techniques influenced the graphene nanoplatelet geometry which reduced the aspect ratio of the platelets. The results showed that by incorporating 2 wt% graphene into the epoxy matrix, combined with a multilayer fabrication method, reduced the helium gas permeability by 83% when compared to the reference epoxy samples. Modelling the gas permeability

according to the tortuous path theory confirmed the aspect ratios which were estimated by the microscopic methods and particle size analysis.

\*Corresponding author, e-mail address: [louis.vanrooyen@necsa.co.za](mailto:louis.vanrooyen@necsa.co.za), Tel. number: (+27) 12 305 6123, Fax number: (+27) 12 305 6377

## 1 Introduction

Graphite moderated nuclear reactors have been operational since the mid-20<sup>th</sup> century and some are already in the process of being decommissioned and many still need to be decommissioned because they are now reaching the end of their proposed operational service life. From the decommissioning process of these reactors, large volumes of irradiated graphite waste will be generated which is estimated to be in the region of 250 000 tonnes and will require safe immobilisation and appropriate disposal methods [1,2]. The irradiated graphite waste generated from this decommissioning process contains radionuclides which are produced due to the neutron activation of impurities present in the graphite [1,3,4]. The main problematic radionuclides present in the irradiated graphite are tritium (<sup>3</sup>H), carbon-14 (<sup>14</sup>C), and chlorine-36 (<sup>36</sup>Cl). These problematic radionuclides are released over time due to diffusion from the graphite structure in gaseous form (<sup>3</sup>H<sub>2</sub>, <sup>14</sup>CO<sub>2</sub>, <sup>14</sup>CH<sub>4</sub>, and <sup>36</sup>Cl<sub>2</sub>) with the main activity being produced by the tritium and carbon-14 [5], which will make it difficult to store irradiated graphite waste in confined spaces, like proposed underground storage repositories. Of these radionuclides, tritium gas will most likely permeate faster than the other radioactive gases due to its small molecular size.

Polymers are being researched as a viable option to immobilise low level irradiated graphite waste from gas-cooled graphite moderated nuclear reactors after being dismantled due to their versatile properties when compared to more traditional methods like Portland cements [3,6]. The impregnation of this waste with epoxy resin

can be effective in limiting the leaching of radionuclides from the graphite structure [7,8]. However, most polymers tend to exhibit poor gas barrier properties when compared to other materials like metals [9–11]. Therefore, radioactive gases like tritium can easily permeate through these polymeric structures over time, which poses the threat of accumulation in underground repositories.

Fortunately, these properties can be improved by the incorporation of fillers which possess a platelet-like geometry and high aspect ratio [12]. Through the incorporation of nano-sized particles into a pure polymer matrix, and through proper dispersion and orientation of these particles, significant reduction of the gas permeability can be achieved [12–28]. These fillers create a tortuous path or maze which restricts the migration of the diffusing gas molecules through the polymer matrix by increasing the path length.

Graphene exhibits this platelet structure and has recently attracted a lot of interest in the field of barrier applications due to its unique property enhancement ability [17,19,29,30]. Graphene nanoplatelets are impermeable to gases such as helium if the platelets contain no defects [31–33] and is already being applied in coatings as barriers against the release of toxic substances [31,34]. If this is the case, then graphene nano-polymer composite coatings might be useful in limiting the release of radioactive gases like tritium ( $^3\text{H}$ ) from irradiated graphite waste.

In a previous study done, glass flake filled epoxy showed promising results as a possible barrier coating to limit or prevent the release of tritium gas [4]. The advantage that graphene nanoplatelets possess over glass flakes is that the aspect ratio is significantly higher which according to theory should make the graphene nanoplatelets more effective to reduce the gas permeability with smaller loadings than glass flakes.

However, the effect of settling and agglomeration can seriously limit the effectiveness of the coating to limit or prevent the release of tritium or other radioactive gases if the appropriate coating method is not applied [35]. Graphene nanoplatelets have been observed in practice to settle during gelation of the epoxy resin due to gravity [36,37] and also tend to re-agglomerate due to strong van der Waals forces [38] which can further limit the barrier performance of the composite coating.

Therefore, the aim of this research was to prepare graphene/epoxy nano-composite coatings and determine how the preparation methods would influence the gas permeability of the composite coating. Helium gas was used as a substitute gas for tritium due to safety reasons and also the cost of tritium gas. Helium is similar in size to hydrogen and has been used as a substitute gas to measure the permeation of hydrogen through composite membranes due to helium permeating faster than hydrogen [4,39,40]. Modelling of the helium gas permeability data was done according to the tortuous path theory to determine how the filler loading and dispersion influences the helium gas permeability and diffusion of the graphene/epoxy composite coating.

## **2 Experimental**

### **2.1 Graphene composite coating formulation**

Graphene nanoplatelets in powder form (xGnP grade M-25) were obtained from XG Sciences (USA), with a carbon content of 99.5%, average diameter of 25  $\mu\text{m}$ , and thickness between 6 - 8 nm. The base epoxy resin was a Bisphenol F-based epoxy resin (Araldite LY5082) and the hardener consisted of isophorone diamine (Araldite HY5083) produced by Ciba-Geigy. The resin exhibited a very low viscosity and the gel time is about 3 h, which make it ideal to coat large surfaces such as irradiated graphite from

nuclear reactors. The resin to hardener mixing ratio was 100:23 by weight which corresponds to the stoichiometric ratio.

Graphene platelets, which are similar to carbon nanotubes, are generally dispersed into polymer resins with the use of direct, mechanical, or sonication mixing techniques [37]. Therefore, mechanical mixing with a conventional blender from Russel-Hobbs (700 Watts), ultrasonic mixing with an ultrasonic bath (100 W), and manual mixing by hand were applied to disperse the graphene into the epoxy resin. Incorporation of the graphene nanoplatelets was done according to weight fraction (wt%) of the total resin and hardener system. The loadings of graphene nanoplatelets incorporated into the epoxy resin were at 1, 2, 3, 4, 6, and 10 wt%. Solvent dispersion was considered with loadings above 3 wt% due to the graphene increasing the viscosity of the mixture which prevented the other mixing techniques to be utilised. The solvents used for chemical dispersion of the graphene platelets were dichloromethane (DCM) and tetrahydrofuran (THF) obtained from Sigma Aldrich, Germany and N, N-dimethyl formamide (DMF) from Associated Chemical Enterprises, South Africa.

## **2.2 Permeation sample preparation**

### **2.2.1 General**

The doctor blade<sup>1</sup> sheets were prepared at an approximate thickness of 2 mm and the moulded discs and multilayer sheets at an approximate thickness of 4 mm. Disc permeation specimens with a diameter of 45 mm were machined from the doctor blade and multi-layered sheets to fit the permeation cell, whereas the moulded disc specimens

---

<sup>1</sup> Doctor blades are used in paint and ceramic technology to prepare thin films and to evaluate the degree of dispersion of additives like pigments. A doctor blade works on the principle that a substrate (normally glass, metal, or plastic) is moved under a blade with an adjustable height, from a stationary position, to produce a thin film or sheet (Aegerter, M.A., Mennig, M., 2004. Sol-gel technologies for glass producers and users. Springer. pp 89-92)

were moulded in polyethylene moulds with a diameter of 45 mm. Reference Araldite epoxy resin samples were prepared as doctor blade sheets and moulded discs to compare the helium gas permeability of the composite samples to unfilled epoxy resin, by mixing 100 g of epoxy with 23 g of hardener by hand for 2 min whereafter the appropriate sheet and disc samples were prepared.

### **2.2.2 Doctor blade sheets**

Sheets were prepared with graphene loadings incorporated into 100 g of epoxy resin. Mechanical, ultrasonic, and manual mixing were used to incorporate 1 wt% loadings while mechanical mixing was used to incorporate 2 and 3 wt% loading of graphene platelets. After mixing, 23 g of hardener was stirred in by hand for 2 min. The composite mixture was poured on polyethylene sheets and dragged under the Meier blade to get a uniform sheet thickness of 2 mm. The sheets were left for 7 days to cure at room temperature.

### **2.2.3 Moulded discs**

Moulded discs were prepared with the aid of solvent mixing to incorporate higher loadings of graphene nanoplatelets. The loadings of graphene nanoplatelets incorporated were 4, 6, and 10 wt%. The graphene nanoplatelets were initially dispersed in 50 ml of a selected solvent using ultra-sonication for 20 min and then mixed into 100 g of the epoxy resin. The composite/solvent mixture was further sonicated for 2 h at 50 °C. The solvent was evaporated off with a Buchi rotary evaporation system, allowed to cool and hardener was added and stirred for 2 min. The composite mixture was then poured into polypropylene moulds and cured in an oven at 50 °C for 15 h.

#### **2.2.4 Multilayer sheets**

The graphene/epoxy composite multilayer sheets were prepared by brushing thin individual layers of graphene epoxy on top of another to create a stacked “sandwich” type structure. The graphene platelets (0.251 g) were dispersed into the epoxy resin (10 g) with a loading of 2 wt% which was sonicated for 5 h at 50 °C. Once cooled and hardener added, a layer would be applied and allowed to dry before another was applied on top of the previous layer until the required thickness of 4 mm was achieved. The sonication mixing with smaller amounts of epoxy resin sufficiently dispersed the graphene nanoplatelets.

#### **2.3 Helium permeation measurements**

In the past few years, helium leak detectors have been regularly utilised as a quick method to determine the gas permeability of various polymers and composite materials [4,9,23,27,28,33,41–45]. The helium gas permeation flux was measured using a specially designed permeation cell which was attached to a Leybold L200+ helium leak detector which could only detect a minimum helium flux measurement of  $2.3 \times 10^{-12} \text{ mol.m}^{-2}.\text{s}^{-1}$ . Afrox (African Oxygen Limited) helium 5.0 (99.999%) gas was used as the permeation test gas. The helium gas flow into the top part of the permeation cell was verified with a gas flow meter at  $50 \text{ ml.min}^{-1}$ , with the bottom part being evacuated with the vacuum pump unit in the helium leak detector to create a pressure differential on the opposite end of the composite membrane. All measurements were performed up to 28 000 s at 295 K. A detailed description of the permeation setup and cell is given in [4].

The helium leak rate ( $J^*$ ) of the graphene/epoxy coatings was measured in  $\text{mbar.l.s}^{-1}$  but converted to  $\text{Pa.m}^3.\text{s}^{-1}$  as to calculate the helium gas flux ( $J$ ,  $\text{mol.m}^{-2}.\text{s}^{-1}$ ) from the following equation:

$$J = \frac{J^*}{ART} \quad (1)$$

Where,  $A$  is the surface area ( $0.0013 \text{ m}^2$ ),  $R$  the gas constant ( $8.315 \text{ J.K}^{-1}.\text{mol}^{-1}$ ) and  $T$  the temperature ( $295 \text{ K}$ ).

#### **2.4 Composite structure and graphene nanoplatelet characterisation**

The graphene epoxy composite morphology was evaluated by the use of microscopy, X-ray diffraction, and Microfocus X-ray tomography techniques. High resolution Scanning Electron Microscopy (SEM) imaging was performed on a JEOL JSM-6380LA Field Emission Gun (FEG) SEM to give an indication of the degree of dispersion of the graphene nanoplatelets in the epoxy resin. The samples were viewed at a beam intensity of 20 kV and were sputter coated with gold to improve the imaging quality. Transmission electron microscopy (TEM) was performed with a JEOL-Jem 2100 with a beam intensity of 200 kV to evaluate the shape and form of the graphene platelets in the epoxy resin. Ultra-thin sections of the graphene/epoxy nanocomposite samples were cut to a thickness of 50-70 nm using a Leica EM UC6 ultra-microtome and a Diatome diamond knife at room temperature. The prepared sections were collected on a 200 mesh copper (Cu) grid for viewing with the TEM. Calibrated images were captured electronically with a Gatan Ultrascan camera and Digital Micrograph software. Micro-focus X-ray tomography was performed on a Metris XT H 225L to determine the degree of dispersion and arrangement of the graphene nanoplatelets in the epoxy resin [46].

Wide angle X-ray diffraction (WAXD) was conducted on sampled sections from the prepared sheets to determine how the mixing techniques influenced the structure formation and dispersion of the graphene nanoplatelets in the composite structure. The analysis was performed with a Bruker D8 advance diffractometer from Bruker scanning the samples in  $2\theta$  range between  $15$  and  $30^\circ$  at a stepsize of  $0.04^\circ$  using  $\text{Cu K}\alpha$  irradiation at  $40$  kV.

Particle size analysis was performed on the graphene nanoplatelets using a Micromeritics Saturn Digisizer II particle size analyser. The graphene nanoplatelets ( $0.025$  g) were dispersed in  $20$  cm<sup>3</sup> isopropanol (ACE) and Triton X (Sigma Aldrich) was used as a dispersing agent. Thereafter, the prepared samples were sonicated for specific time intervals and the samples added drop wise into the instrument to obtain an obscuration of  $18\%$  to perform measurements.

Atomic Force Microscopy (AFM) was performed with a modified Digital Instruments Nanoscope, Veeco, MMAFMLN-AM (Multimode) AFM at the National Centre for Nanostructured Materials based at the Council for Scientific and Industrial Research (CSIR, South Africa) to determine the platelet thickness of the graphene nanoplatelets. The tapping mode was used to probe the deposited graphene nanoplatelets at ambient temperature of  $23$  °C. The graphene nanoplatelets were deposited on silicon wafers after being dispersed in chloroform by sonication for  $30$  min and manual stirring by hand.

## **3 Results and discussion**

### **3.1 Mixing techniques**

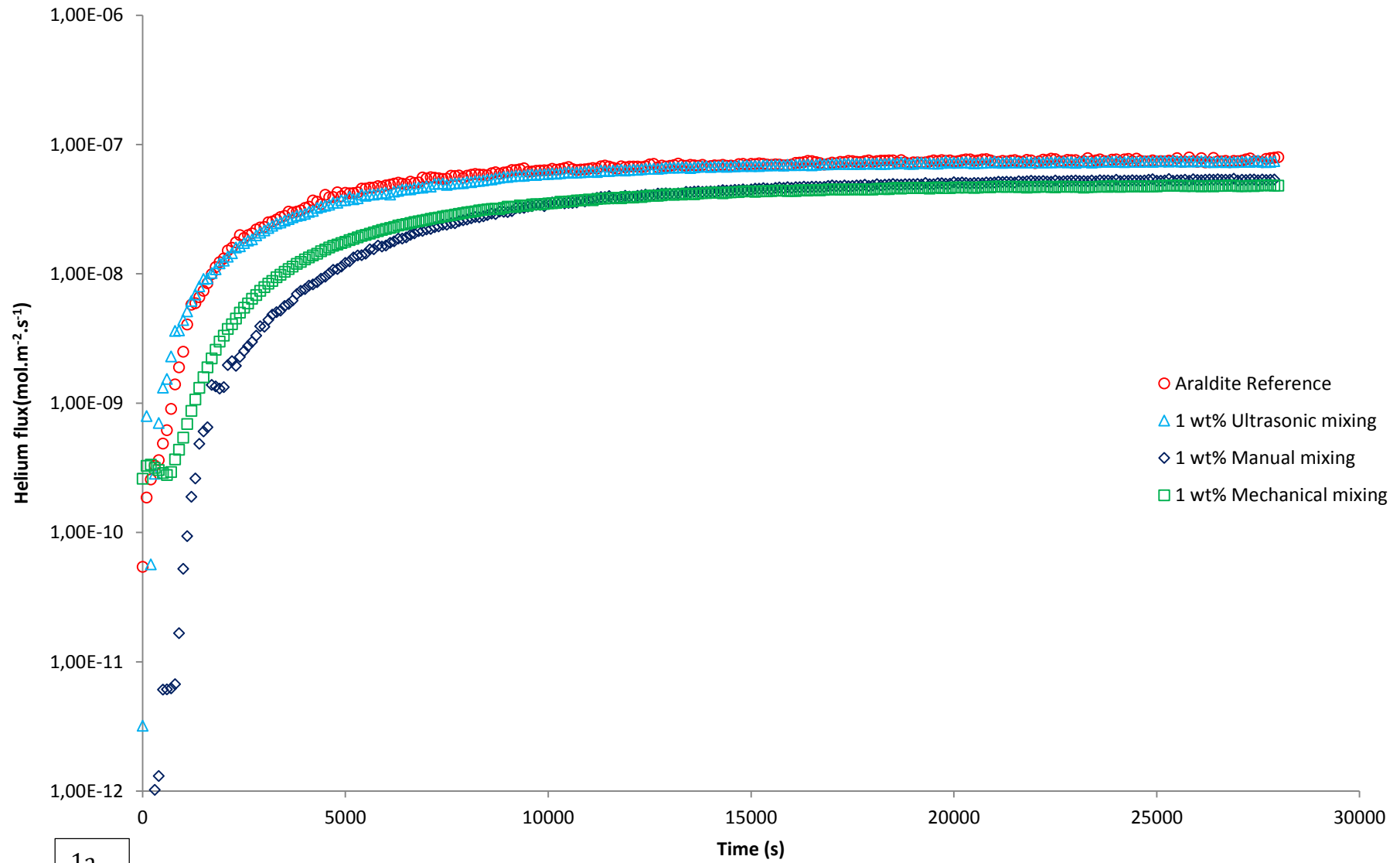
The mixing techniques and coating preparation methods were chosen in order to reflect real-world conditions and to determine whether the composite coatings could act as an efficient gas barrier. Normally, coating formulations would be prepared under ideal laboratory conditions to achieve optimum performance, but this might not suffice in practice when applied to large areas of irradiated graphite waste. Therefore, the graphene/epoxy composite samples were prepared as doctor blade sheets, moulded discs, and multilayer sheets as to reflect the same features of a resin coated on a substrate. With increased loadings the viscosity of the graphene epoxy mixtures also increased due to the low bulk density of the graphene nanoplatelets. This was the main limitation with each mixing technique to disperse the graphene platelets in the epoxy resin.

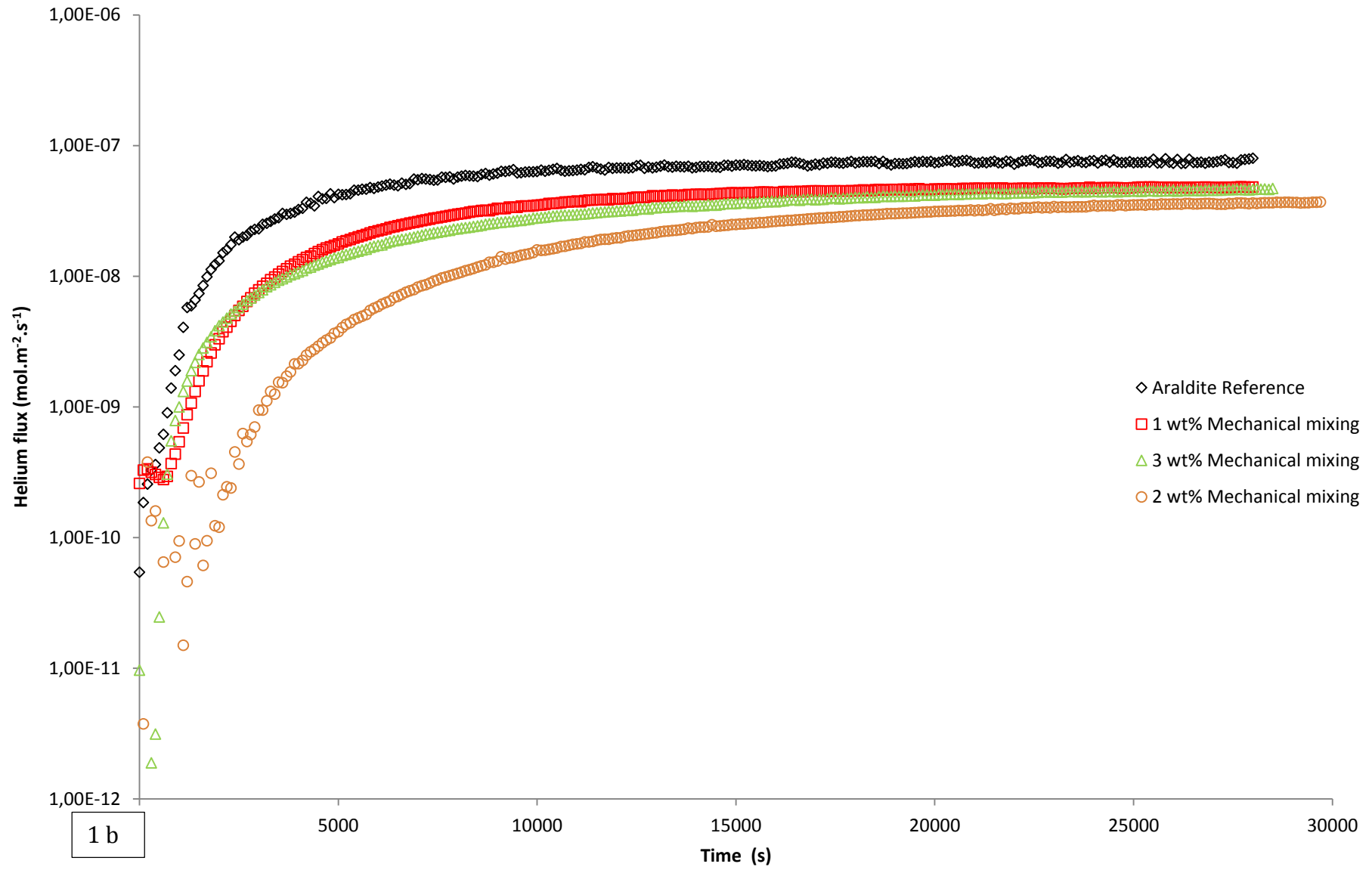
### **3.2 Helium permeability of coatings**

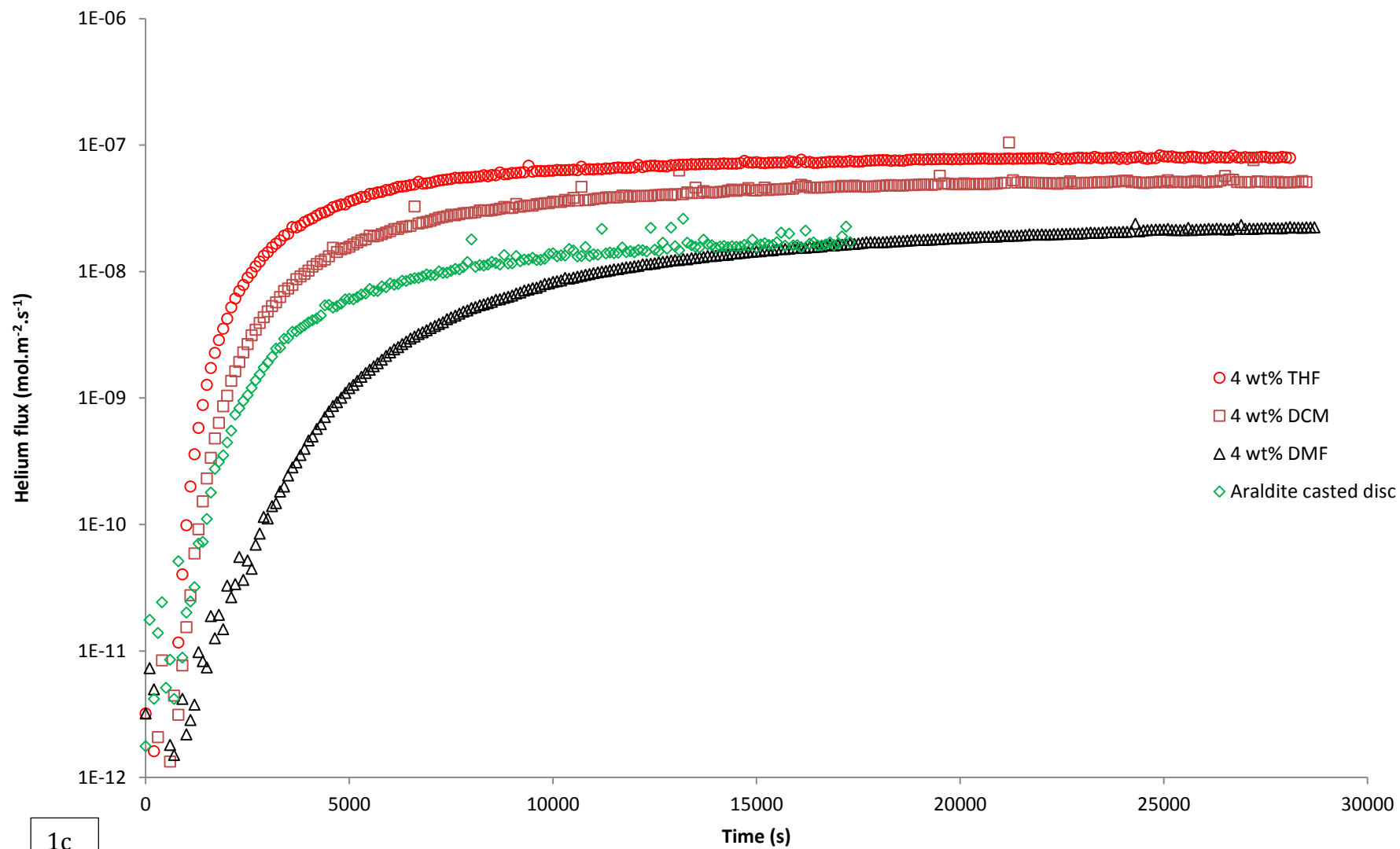
#### **3.2.1 Permeation measurements**

##### ***3.2.1.1 Doctor blade sheets***

Permeation experiments were performed on doctor blade samples with concentrations of 1 wt% graphene nanoplatelets which were dispersed by mechanical, ultrasonic, and manual mixing. From the helium permeation results it can be clearly seen that for most of the samples, the incorporation of graphene nanoplatelets into the epoxy matrix reduced the helium permeation when compared to the pure epoxy matrix (**Fig 1**).







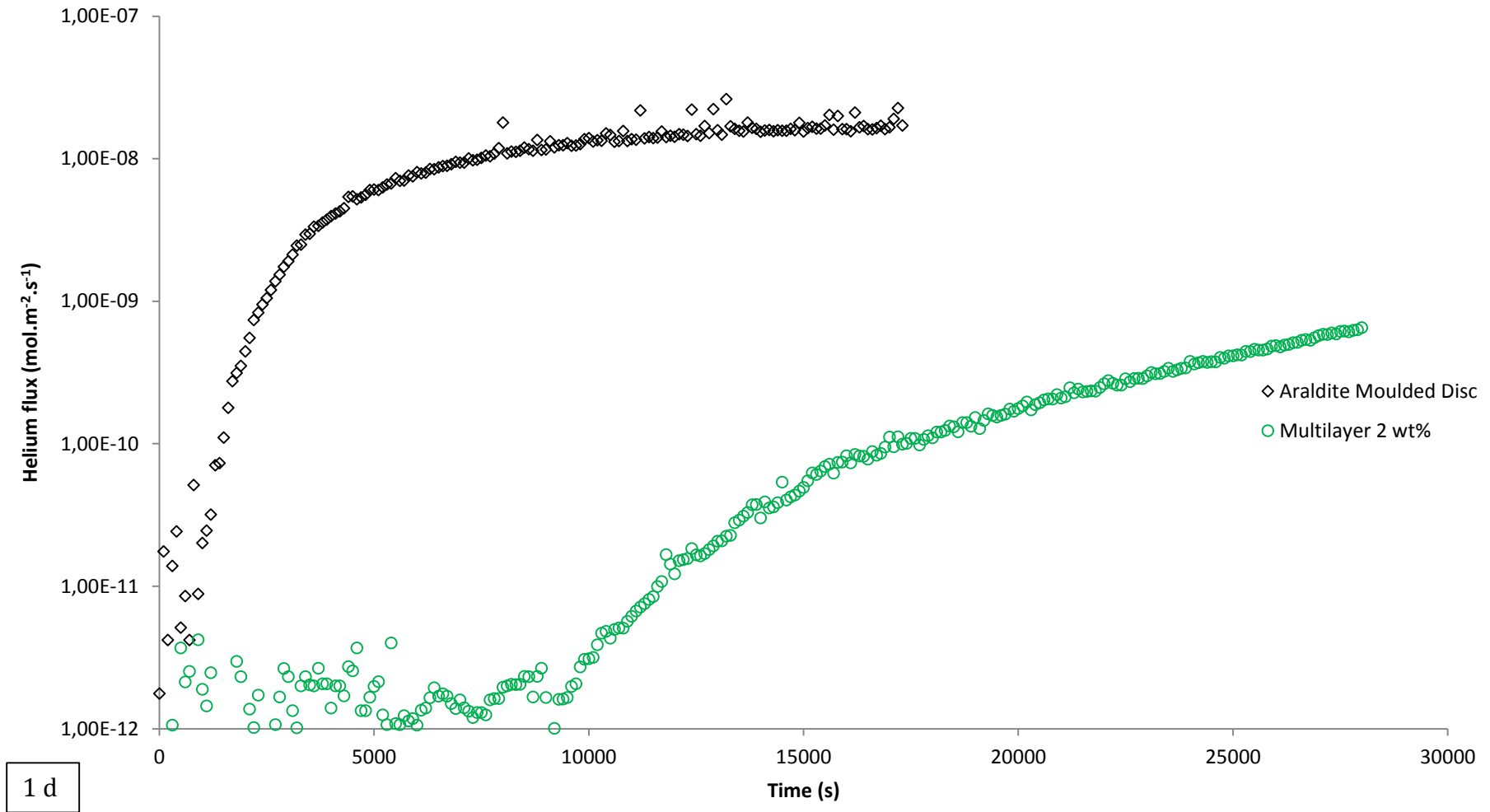


**Figure 1:** Helium flux measurements of the doctor bladed samples filled with (a) 1 wt% graphene nanoplatelets and the (b) mechanically dispersed sheets, (c) moulded discs with higher loadings of graphene nanoplatelets, and the (d) multilayer sheet.

However, the dispersion method applied also influenced the efficiency in reducing the helium permeation as noticed with the mechanical and manual mixing techniques reducing the helium permeation more than the ultrasonic dispersion for 30 min (**Fig 1a**). Examination of the composite coating morphology by SEM further showed that the doctor blade sheet (1 wt%) which used sonication to disperse the graphene nanoplatelets exhibited highly agglomerated regions and settling which confirmed why the sheet showed very little reduction of the helium permeation (**Fig 2**). This re-agglomeration of the platelets compromised the barrier structure and hence no significant reduction was observed. The length of the sonication time was most likely insufficient to cause adequate separation of the graphene nanoplatelets. The manual mixing method showed a surprising result as this method was expected to perform the worse out of the three mixing techniques, but reduced the helium permeation almost the same as the mechanical mixing method.

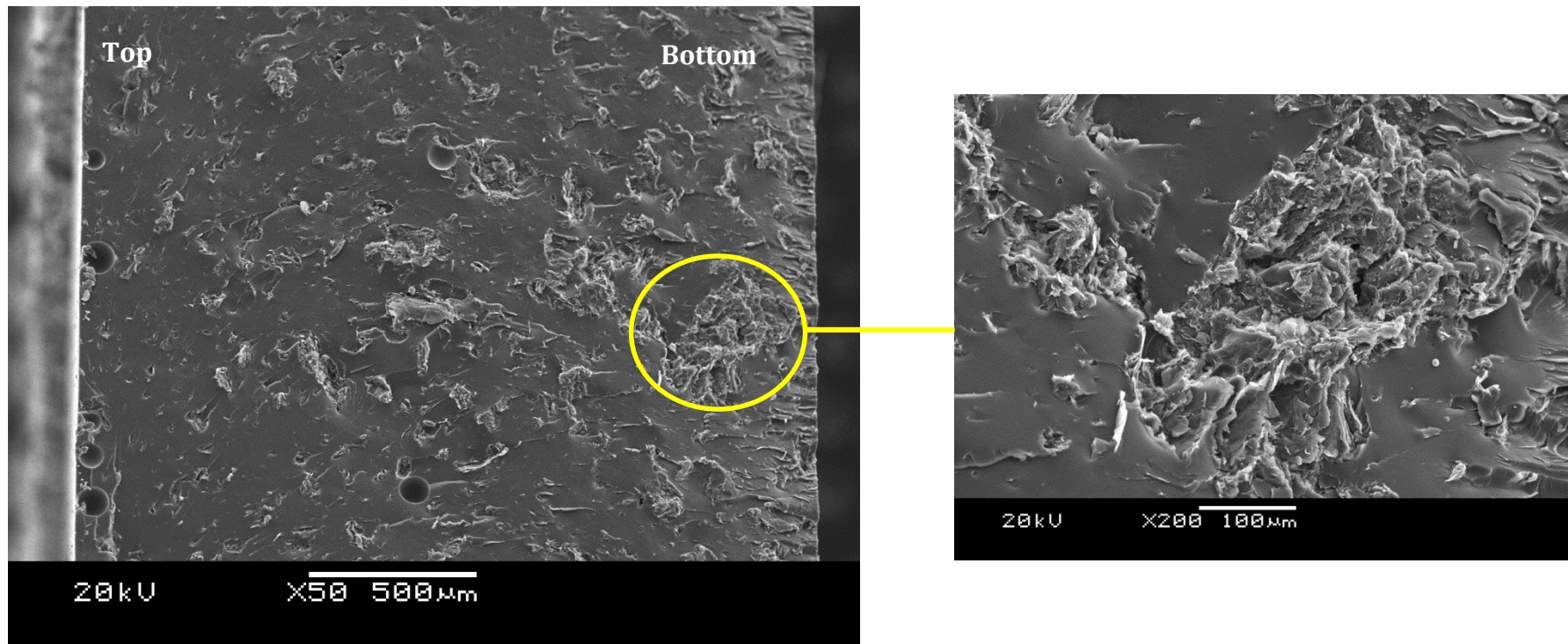


**Figure 2:** SEM image of the doctor blade sheet morphology which was prepared by ultrasonic dispersion with the highly agglomerated area further magnified.

Above 1 wt% loading, using the manual and ultrasonic mixing methods, we were unable to disperse the graphene nanoplatelets, with only the blender managing up to 3 wt% loading. The loading of 2 wt% exhibited the best reduction of the helium permeation for the doctor blade sheets which appeared to be the percolation threshold seeing that from the 3 wt% loading the helium permeation began to increase slightly (**Fig 1b**). The mechanical mixing produced better dispersion of the graphene nanoplatelets with random orientation, but it also appeared to have reduced the size of the graphene platelets (**Fig 3**).

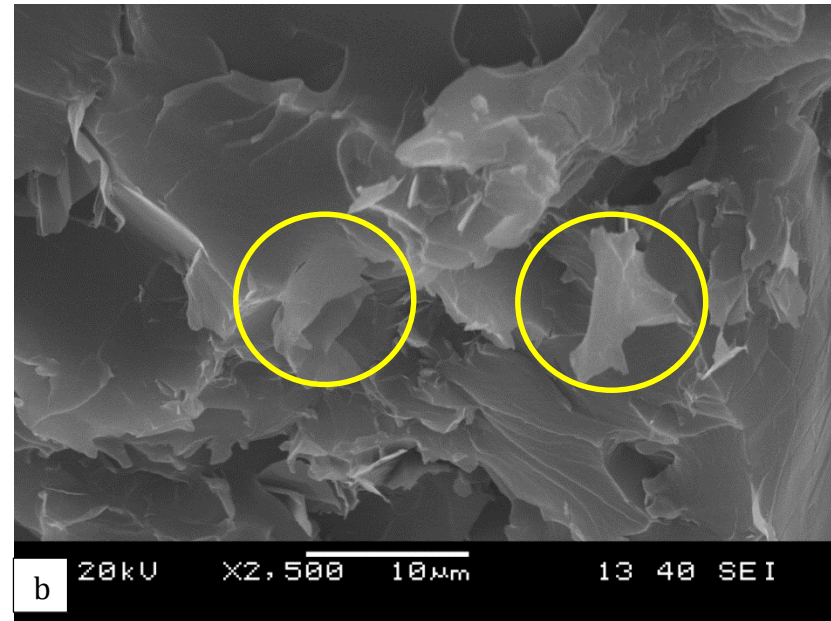
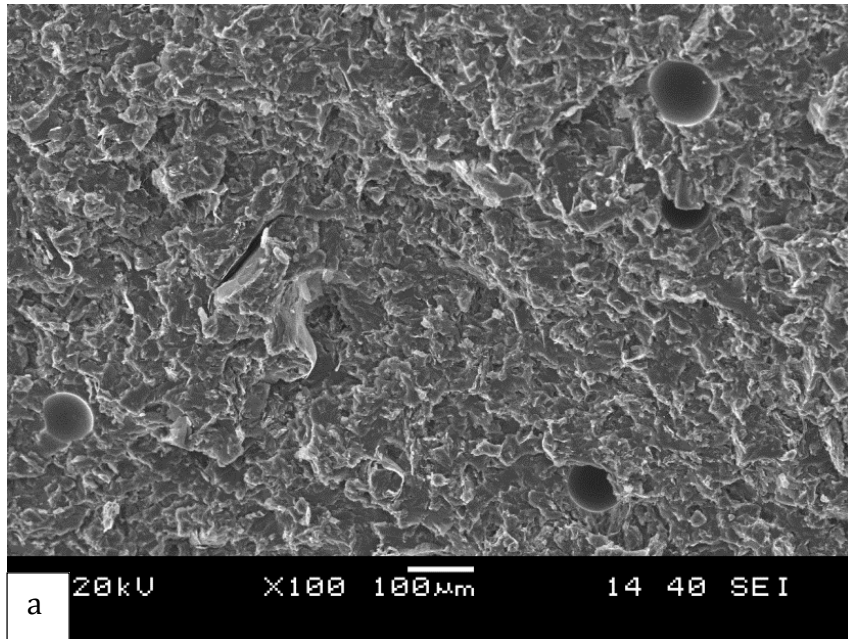


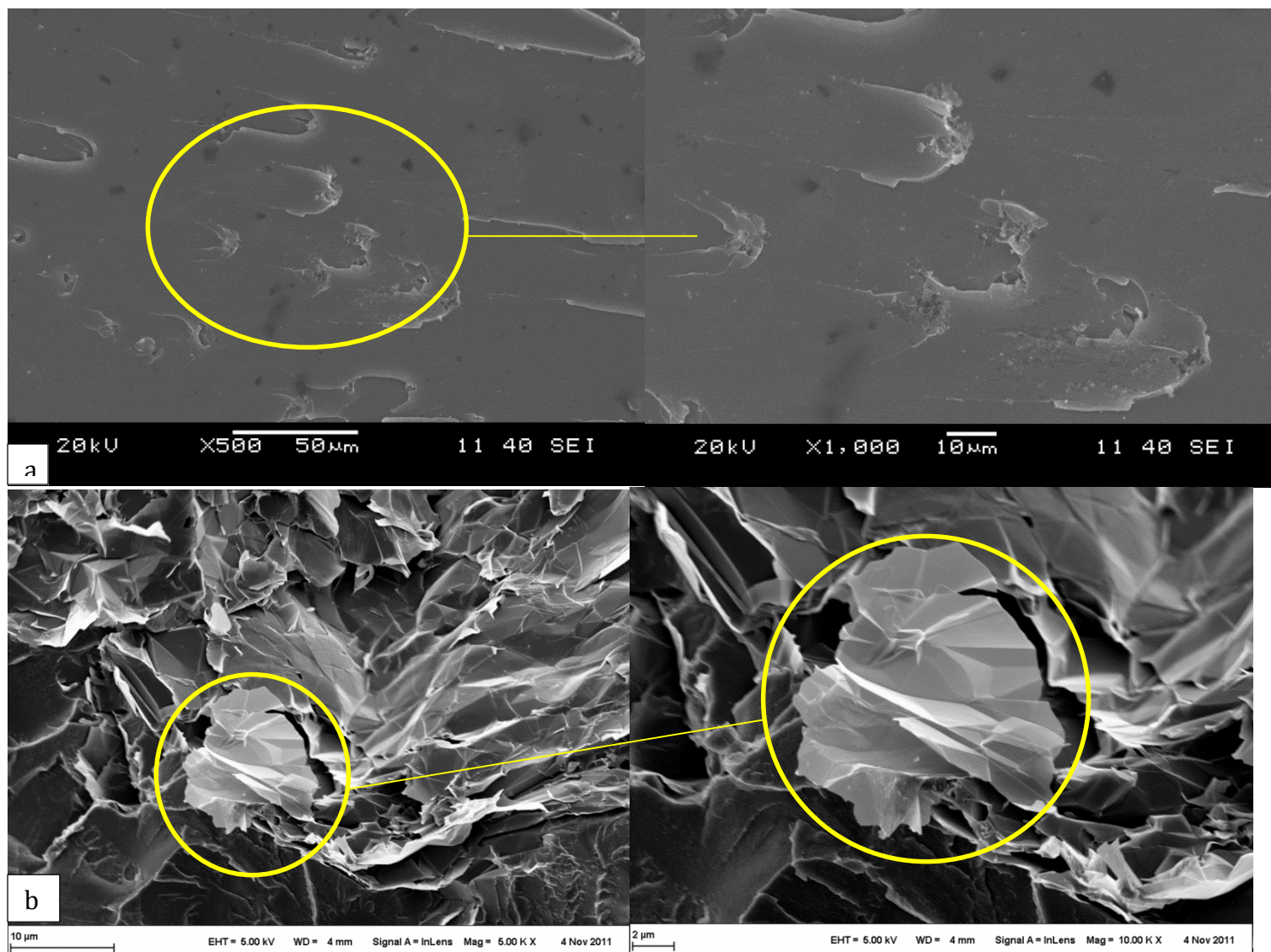
**Figure 3:** SEM images of (a) mechanical mixed doctor blade sheet (2 wt%) morphology and (b) graphene platelet size reduction indicated in yellow area

### **3.2.1.2 Moulded discs**

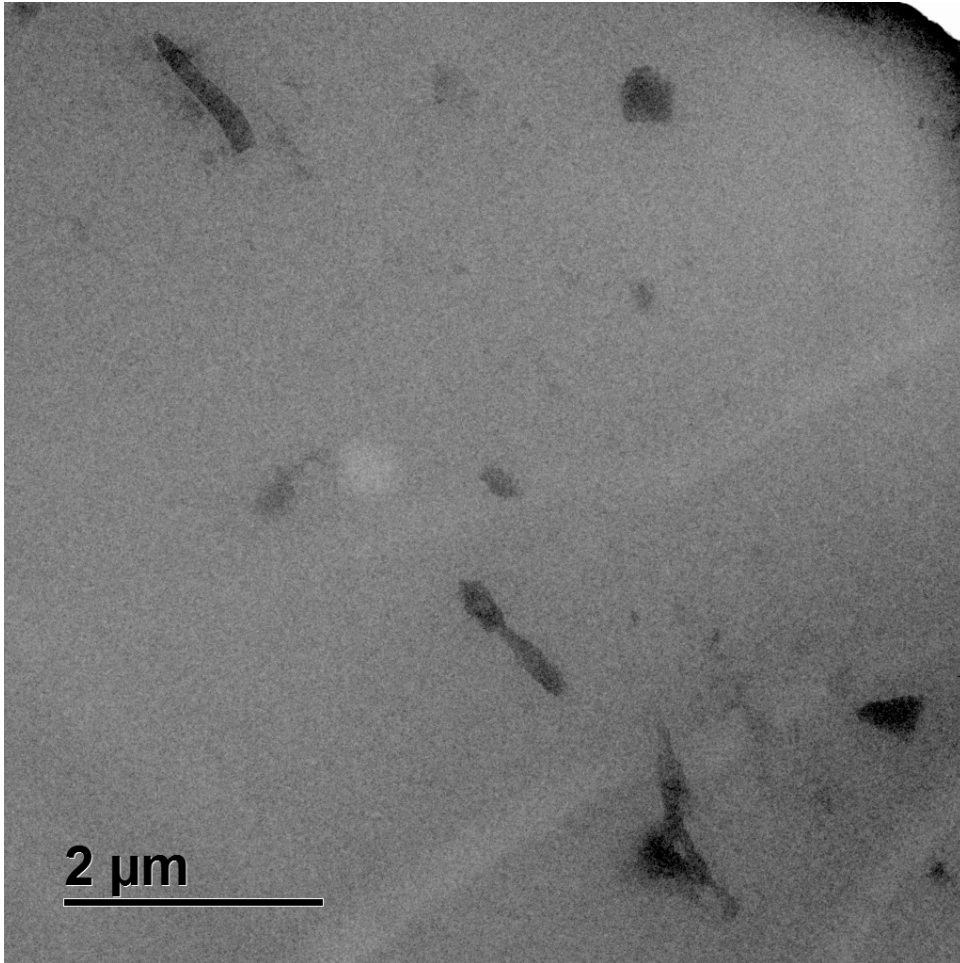
Moulded disc samples were prepared with the aid of solvents to incorporate higher loadings of graphene nanoplatelets at 4, 6, and 10 wt% due to the mechanical, ultrasonic and manual mixing techniques not being able to mix such high loadings. Permeation tests could not be performed on the moulded disc samples which were prepared at 6 and 10 wt% loadings due to the samples being too porous so that the helium leak detector was unable to achieve proper vacuum to initiate any measurements. With the evaluation of the 4 wt% disc samples the helium permeation increased when compared with the epoxy reference sample, which may be attributed to the use of solvents adversely affecting the curing of the epoxy resin (**Fig 1c**).

### **3.2.1.3 Multilayer sheet**

Incorporation of 2 wt% graphene platelets into the epoxy resin showed to be a good loading to reduce the helium permeation and therefore, a loading of 2 wt% graphene nanoplatelets was selected to prepare the multilayer sheets. The multilayer sheet samples reduced the helium permeation an order of magnitude more than the reference sample (**Fig 1d**). The SEM images of the multilayer sheet morphology, which also used sonication to disperse the platelets, showed that the platelets were better dispersed and smaller than 10  $\mu\text{m}$  (**Fig 4**). This was confirmed with TEM images which also showed that the particles were smaller than 10  $\mu\text{m}$  and even went down to 2  $\mu\text{m}$  (**Fig 5**). This indicated that longer sonication times not only helped with improving the dispersion, but further reduced the size of the graphene nanoplatelets.

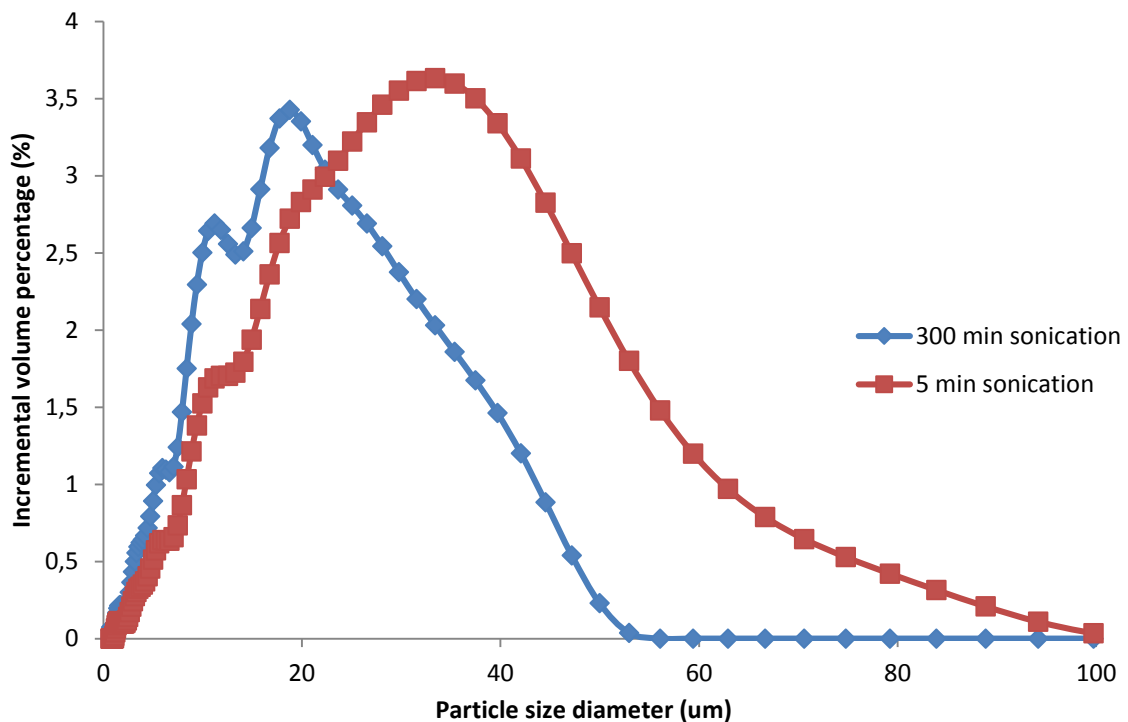


**Figure 4:** SEM images of the (a) 2 wt% multilayer sheet morphology showing (b) graphene platelets with an approximate diameter of 10 µm



**Figure 5:** TEM image of the 2 wt% multilayer sheet showing dispersed particles smaller than 10  $\mu\text{m}$

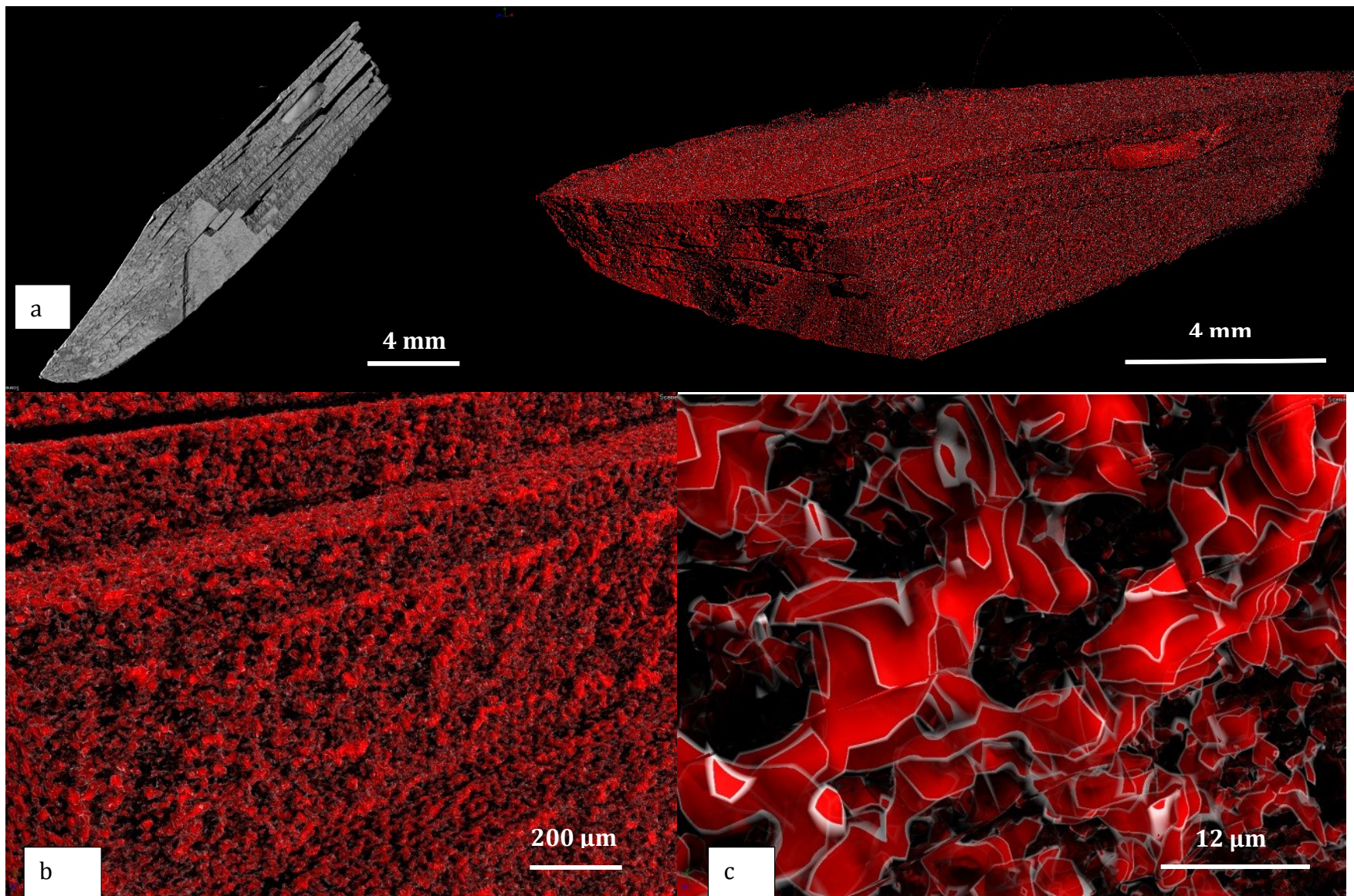
To confirm whether this was the case, particle size analysis was performed on the graphene nanoplatelets (**Fig 6**) and it could be seen that with longer sonication times the particle size does become smaller compared to the graphene nanoplatelets dispersed at shorter times. This variation in particle size was also observed by Chong and Taylor [47].



**Figure 6:** Particle size analysis performed on graphene nanoplatelets dispersed in IPA showing how the particles become finer with extended periods of sonication.

Due to the density difference between the graphene and epoxy matrix, the graphene nanoplatelets could be attenuated to show how the platelets were dispersed in the epoxy matrix of the multilayer sample with the aid of microfocus x-ray tomography (**Fig 7a**). From the observation it could be seen that the nanoplatelets were well dispersed in the epoxy matrix and exhibit a random orientation with respect to the permeation direction (**Fig 7b-c**). Measuring the size of some of the particles confirmed

that the particles became smaller as was observed with the SEM and TEM imaging of the multilayer sample (**Fig 7d**).



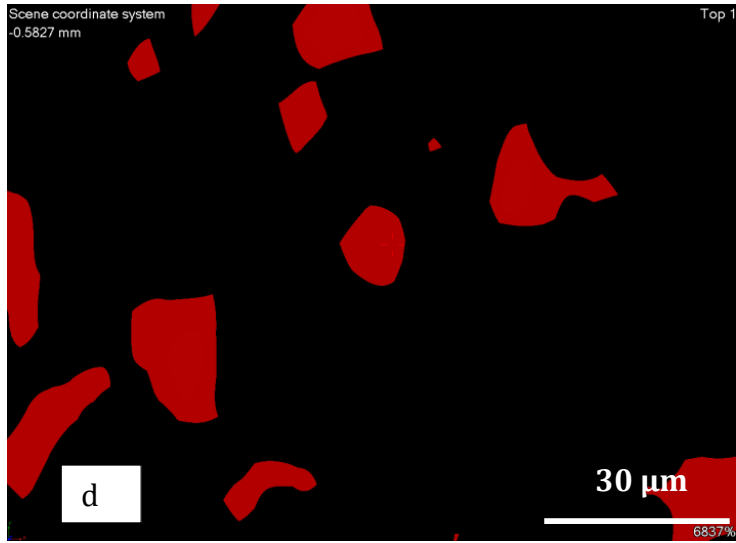


Figure 7: X-ray tomogram showing a section of the (a) multilayer sample and the attenuated graphene nanoplatelets dispersed in the matrix. Closer view of some of the (b) individual layers and (c) the graphene nanoplatelets in the multilayer sheet. (d) Measurements of the platelets in 2-dimensional perspective.

### 3.2.2 Determining the diffusion and permeability coefficients

To determine the helium gas diffusion ( $D$ ) coefficients and steady state flux ( $J_0$ ) of the graphene/epoxy nanocomposites the following one-dimensional variation of Fick's law of diffusion was applied with the appropriate boundary conditions [4,13,23,45,48]:

$$J = J_0 \sqrt{\frac{4d^2}{\pi Dt}} \sum_{x=0}^{\infty} \exp \left[ -\frac{d^2}{4Dt} (2x + 1)^2 \right] \quad (2)$$

where  $J$  is the calculated helium gas flux and  $J_0$  is the steady-state helium gas flux ( $\text{mol.m}^{-2}.\text{s}^{-1}$ ),  $d$  is the sample disc thickness (m),  $t$  the time (s), and  $D$  is the diffusion coefficient ( $\text{m}^2.\text{s}^{-1}$ ).

In the earlier stages of gas diffusion, Equation 2 can be simplified to the following form as an approximation:

$$J \cong J_0 \sqrt{\frac{4d^2}{\pi Dt}} \exp \left( -\frac{d^2}{4Dt} \right) \quad (3)$$

The diffusion coefficient ( $D$ ) and the steady-state helium flux ( $J_0$ ) were graphically determined by plotting the linear form (Equation 4);  $\ln(J\sqrt{t})$  against  $1/t$  and fitting the results to a linear trend line [4].

$$\ln(J\sqrt{t}) \cong -\left(\frac{d^2}{4D}\right) \frac{1}{t} + \ln J_0 \sqrt{\frac{4d}{\pi D}} \quad (4)$$

The helium gas flux measurements from the permeation experiments showed good correlation with the linear fit of Eq 4 with very little statistical deviation which allowed for the accurate calculation of the diffusion co-efficient ( $D$ ), steady-state flux ( $J_0$ ), and the permeability co-efficient ( $P$ ) of the prepared composite samples (**Table 1**). The

helium permeability coefficient ( $P$ , mol.m<sup>-1</sup>.s<sup>-1</sup>.Pa<sup>-1</sup>) was determined from the following equation:

$$P = \frac{J_0 d}{\Delta p} \quad (5)$$

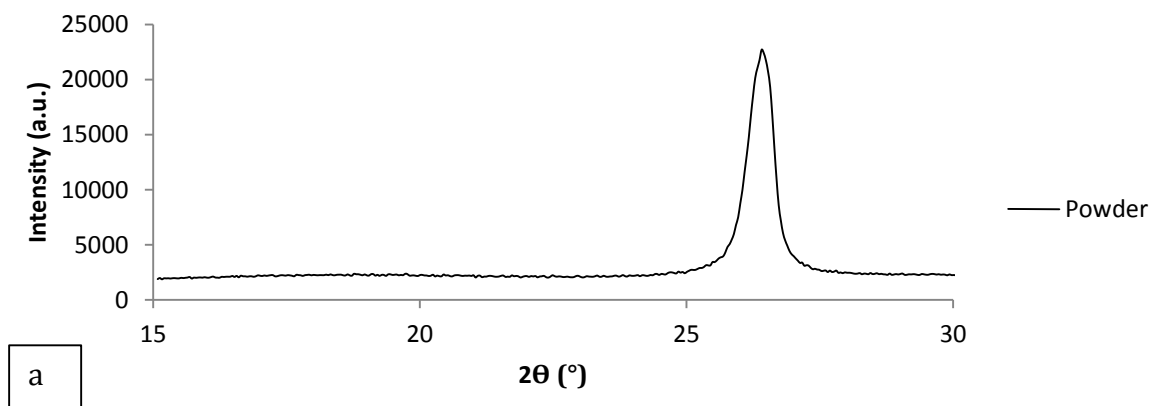
where  $J_0$  is the steady state helium gas flux (mol.m<sup>-2</sup>.s<sup>-1</sup>),  $\Delta p$  is the differential gas pressure (Pa) and  $d$  is the thickness (m) of the composite membrane.

**Table 1:** Calculated values of the permeation flux data according to the one-dimensional Fickian equation

Loading (wt%)	Sample	Mixing method	Steady-state helium flux, $J_0$ (mol.m <sup>-2</sup> .s <sup>-1</sup> )	Diffusion coefficient, D (m <sup>2</sup> .s <sup>-1</sup> )	Permeability coefficient, P (mol.m <sup>-1</sup> .s <sup>-1</sup> .Pa <sup>-1</sup> )	Linear fit (R <sup>2</sup> )
0	Doctor blade	Manual	$7.55 \times 10^{-8}$	$2.49 \times 10^{-10}$	$1.91 \times 10^{-15}$	0.982
1	Doctor blade	Manual	$5.14 \times 10^{-8}$	$0.89 \times 10^{-10}$	$1.28 \times 10^{-15}$	0.991
1	Doctor blade	Ultrasonic	$7.23 \times 10^{-8}$	$1.34 \times 10^{-10}$	$1.76 \times 10^{-15}$	0.976
1	Doctor blade	Mechanical	$4.67 \times 10^{-8}$	$1.27 \times 10^{-10}$	$1.26 \times 10^{-15}$	0.991
2	Doctor blade	Mechanical	$3.73 \times 10^{-8}$	$0.78 \times 10^{-10}$	$1.08 \times 10^{-15}$	0.997
3	Doctor blade	Mechanical	$4.54 \times 10^{-8}$	$0.79 \times 10^{-10}$	$1.14 \times 10^{-15}$	0.991
0	Moulded disc	Manual	$1.76 \times 10^{-8}$	$2.49 \times 10^{-10}$	$1.04 \times 10^{-15}$	0.988
4	Moulded disc	THF	$7.83 \times 10^{-8}$	$5.28 \times 10^{-10}$	$4.04 \times 10^{-15}$	0.995
4	Moulded disc	DCM	$5.02 \times 10^{-8}$	$3.20 \times 10^{-10}$	$2.25 \times 10^{-15}$	0.992
4	Moulded disc	DMF	$2.37 \times 10^{-8}$	$1.17 \times 10^{-10}$	$1.25 \times 10^{-15}$	0.999
2	Multilayer	Ultrasonic	$0.38 \times 10^{-8}$	$0.47 \times 10^{-10}$	$0.18 \times 10^{-15}$	0.990

### 3.2.3 Degree of exfoliation

Analysing the graphene nanoplatelets and the prepared composite sheets with WAXD is a useful technique to determine the degree of exfoliation of the nanoplatelets in the epoxy morphology [36]. The XRD diffraction patterns of the graphene platelets showed a distinct peak at  $2\theta = 26.4^\circ$  which corresponds to the same peak for pure graphite (**Fig 8a**). The patterns for the composite sheets (1 wt%) prepared by mechanical and manual mixing showed a lower intensity peak than the sheets prepared by sonication (**Fig 8b**) which indicate that the graphene platelets were better dispersed with these techniques and hence the reduced helium permeation. Based on the peak position, the d-spacing did not show any significant changes. The pattern of the multilayer sample showed a slight shift in the intensity peak when compared to the mechanical mixing technique with the same concentration (2 wt%)(**Fig 8c**). This suggests that the platelets were slightly better dispersed in the multilayer sample as opposed to the mechanically prepared sample. The amorphous halo, peaked at  $18^\circ$  of  $2\theta$ , is independent in position from both the preparation method and graphene content. This broad peak can be attributed to the formation of small clusters with some molecular orientation therein [49].



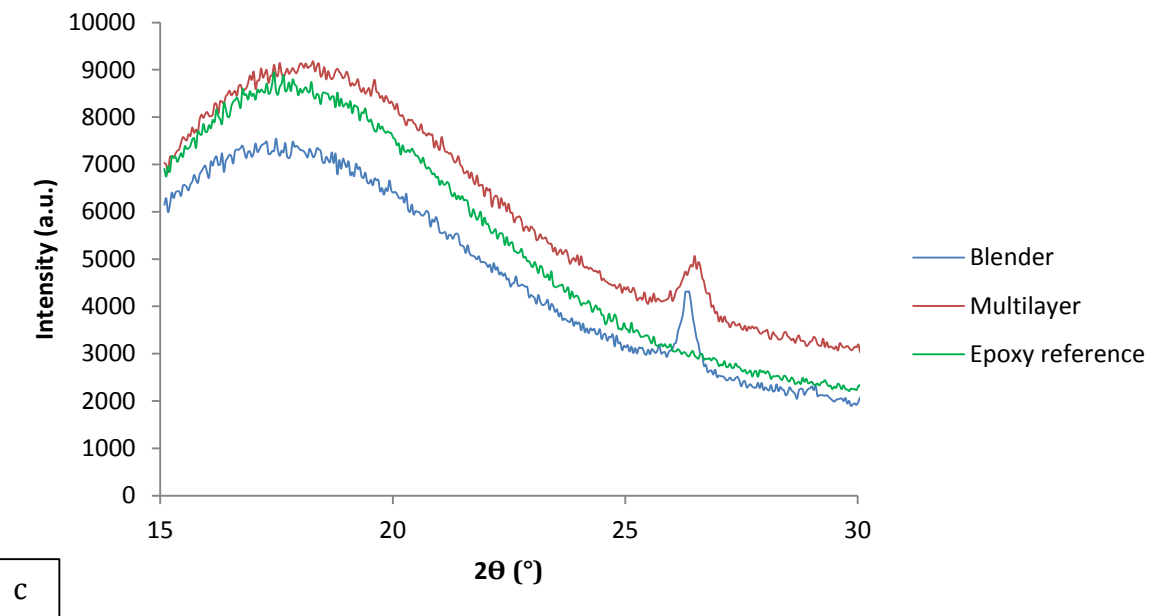
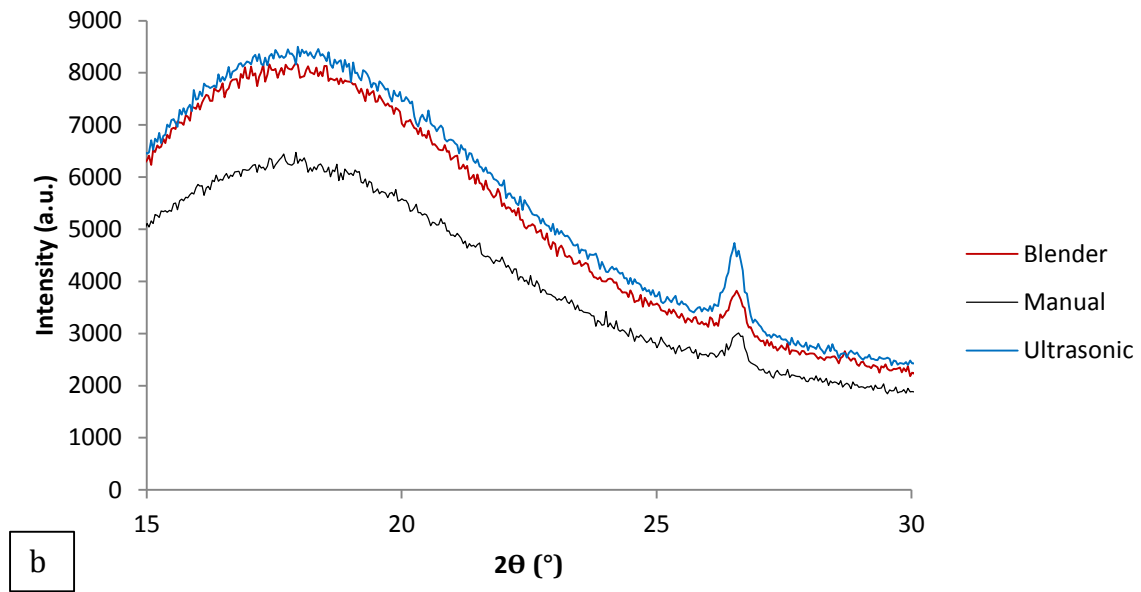


**Figure 8:** X-ray diffraction patterns of (a) the graphene powder and a comparison of the mixing techniques at (b) 1 and (c) 2 wt% graphene concentrations.

### 3.3 Modelling

The relative permeability ( $R_p$ ) was utilised as a normalisation factor due to the different sample preparation techniques that were applied and to determine to what extent the gas permeability was reduced. The  $R_p$  was calculated from the following equation:

$$Rp = \frac{P_c}{P_0} \quad (6)$$

where  $P_c$  is the permeability coefficient of the composite polymer, and  $P_0$  is the permeability coefficient of the pure polymer.

According to the tortuous path theory, the way these particles are dispersed and orientated in the epoxy matrix determines how effectively the nanoplatelets will restrict the movement of the gas molecule through the epoxy matrix. This effectively turns the polymer matrix into a maze which prolongs the diffusion of the gas molecules by increasing the tortuosity factor of the composite polymer matrix if the platelets exhibit high aspect ratios and are properly orientated perpendicularly to the permeation direction.

To describe the effect the tortuous path has on the relative gas permeability ( $Rp$ ), the following equation may be applied:

$$Rp = \frac{P_c}{P_0} = \frac{1 - \phi}{\tau} \quad (7)$$

where  $P_c$  is the permeability coefficient of the composite polymer,  $P_0$  is the permeability coefficient of the pure polymer,  $\phi$  is the nano-platelet loading (expressed in volume fraction), and  $\tau$  is the tortuosity factor. The weight percentage of the composite samples was converted to volume fraction ( $\phi$ ) using the density of the graphene as  $2.2 \text{ g.cm}^{-3}$ .

The tortuosity factors selected for this study are compiled in **Table 2** and have been successfully applied by other researchers to estimate how these nano-platelet fillers influence the gas permeability of polymer composite materials [26,43,50–53]. By substituting the tortuosity factors from the models into Eq 7 the influence of the

nanoplatelets on the relative gas permeability and diffusion coefficient can be estimated. The models that were chosen for this study consider the geometry of the platelets to be ribbons or discs [22,54–57].

**Table 2:** Summary of the tortuosity factors used to model the relative permeability

Model	Filler geometry	Filler dispersion	Aspect ratio	Tortuosity factor ( $\tau$ )
Nielsen [57]	Ribbon	Regular array	w/t	$1 + \frac{\alpha\phi}{2}$
Lape/Cussler-regular array[22]	Ribbon	Regular array	w/t	$1 + \frac{\alpha^2\phi^2}{4}$
Lape/Cussler-random array[22]	Ribbon	Random array	w/t	$\left(1 + \frac{\alpha\phi}{3}\right)^2$
*Bharadwaj[54]	Ribbon	Random array and orientation	w/t	$1 + \left[\frac{\alpha\phi(2S'' + 1)}{6}\right]$
**Fredrickson-Bicerano[55]	Disc	Random array	d/t	$4[(1 + x + 0.1245x^2)/(2 + x)]^2$
Gusev-Lusti[56]	Disc	Random array	d/t	$\exp\left[\left(\frac{\alpha\phi}{3.47}\right)^{0.71}\right]$

\*Factor  $S''$  is incorporated with  $\theta$  being the angle between the obstructing filler and penetrant flow.

$$S = \frac{3\cos^2\theta - 1}{2}$$

\*\*Factor  $x$  is incorporated.  $x = \pi\alpha\phi/[2\ln(\frac{\alpha}{2})]$

The relative permeability of the samples were plotted against the corresponding graphene volume fraction and compared with the model predictions (**Fig 9**). From the results it can be seen that the multilayer technique was the most effective to reduce the helium permeability due to better orientation and dispersion of the graphene nanoplatelets. This technique reduced the helium permeability by 83% when compared to the other dispersion and fabrication techniques (**Table 3**). However, the models did not correlate with any of the relative permeability values of the prepared samples when the theoretical aspect ratio from the supplier's specifications was used (ca 4000).

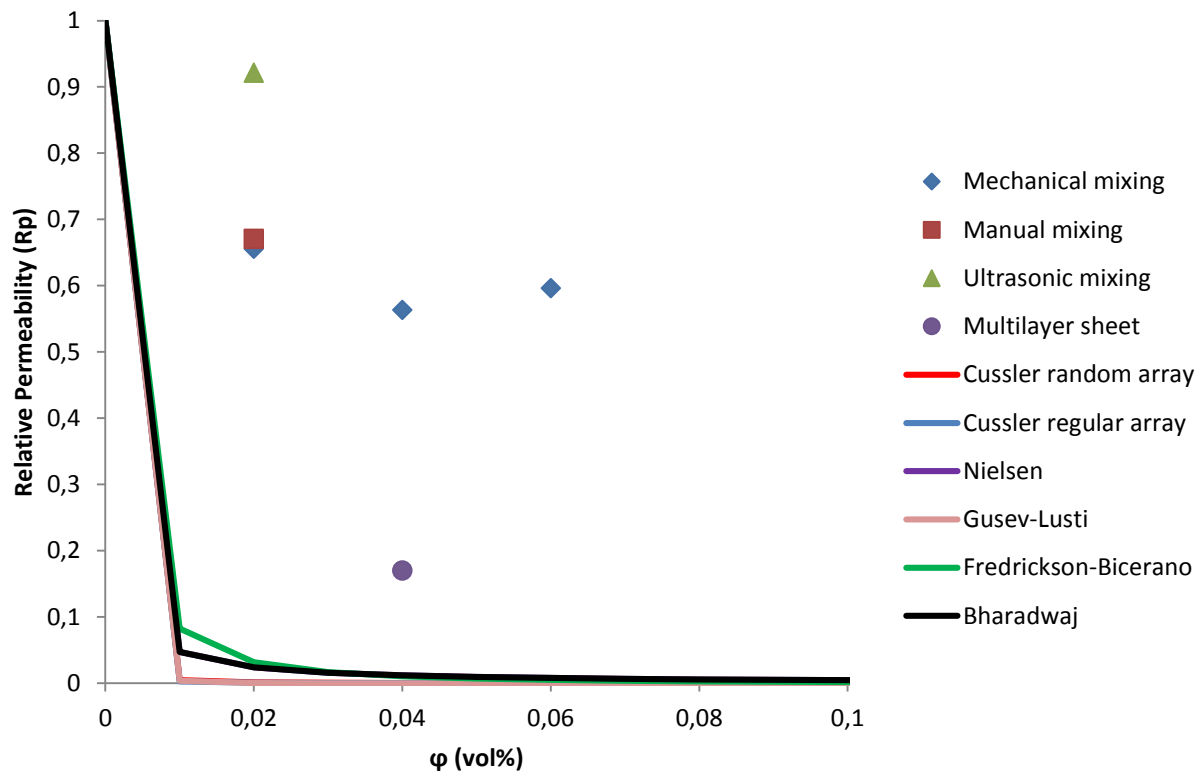


**Figure 9:** Relative permeability values compared to model predictions using the theoretical aspect ratio = ca 4000

**Table 3:** Comparison of the relative helium permeability reduction

Loading (wt%)	Sample	Mixing method	Helium permeability reduction (%)
1	Doctor blade	Manual	32.92
1	Doctor blade	Ultrasonic	7.83
1	Doctor blade	Mechanical	34.44
2	Doctor blade	Mechanical	43.68
3	Doctor blade	Mechanical	40.38
2	Multilayer	Ultrasonic	82.63

Therefore, the thickness of the graphene nanoplatelets was determined with AFM imaging (**Fig 10**). From the AFM measurements (**Table 4**) it showed that the graphene

nanoplatelets which were dispersed with sonication showed better separation of the platelets than manual stirring of the graphene nanoplatelets in the chloroform.

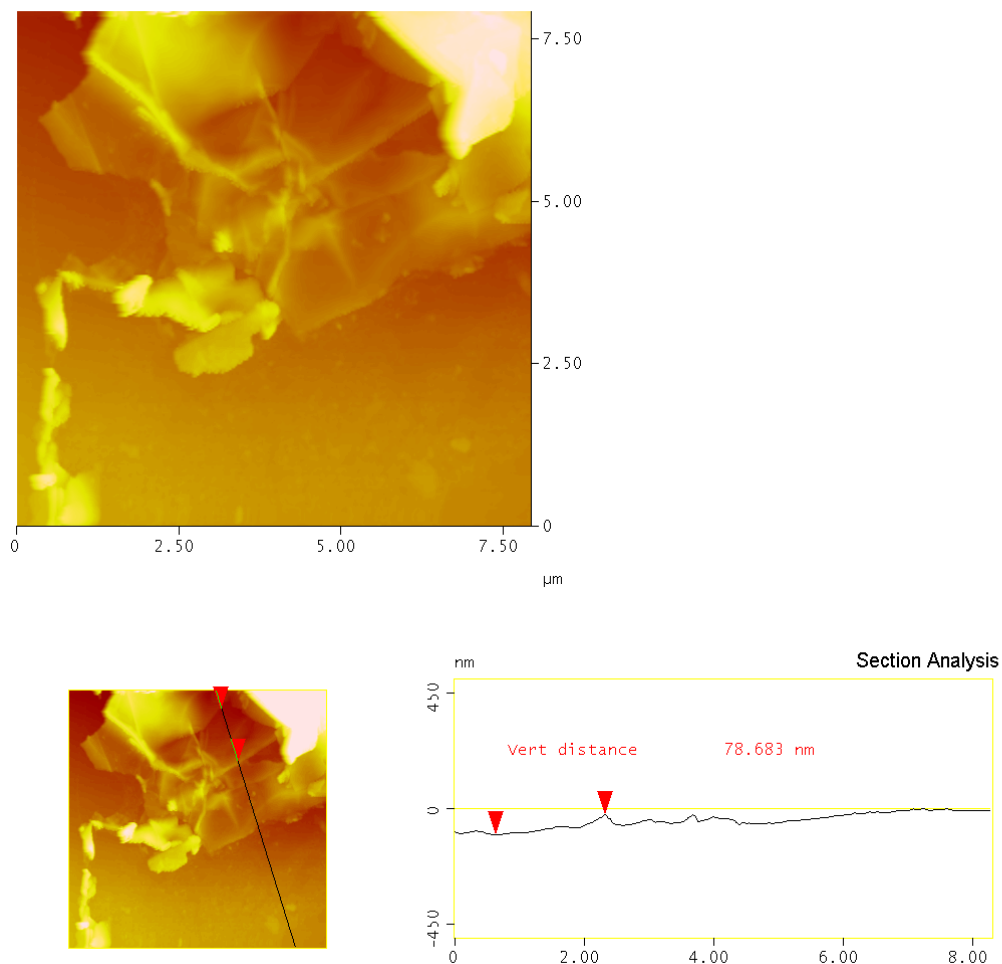


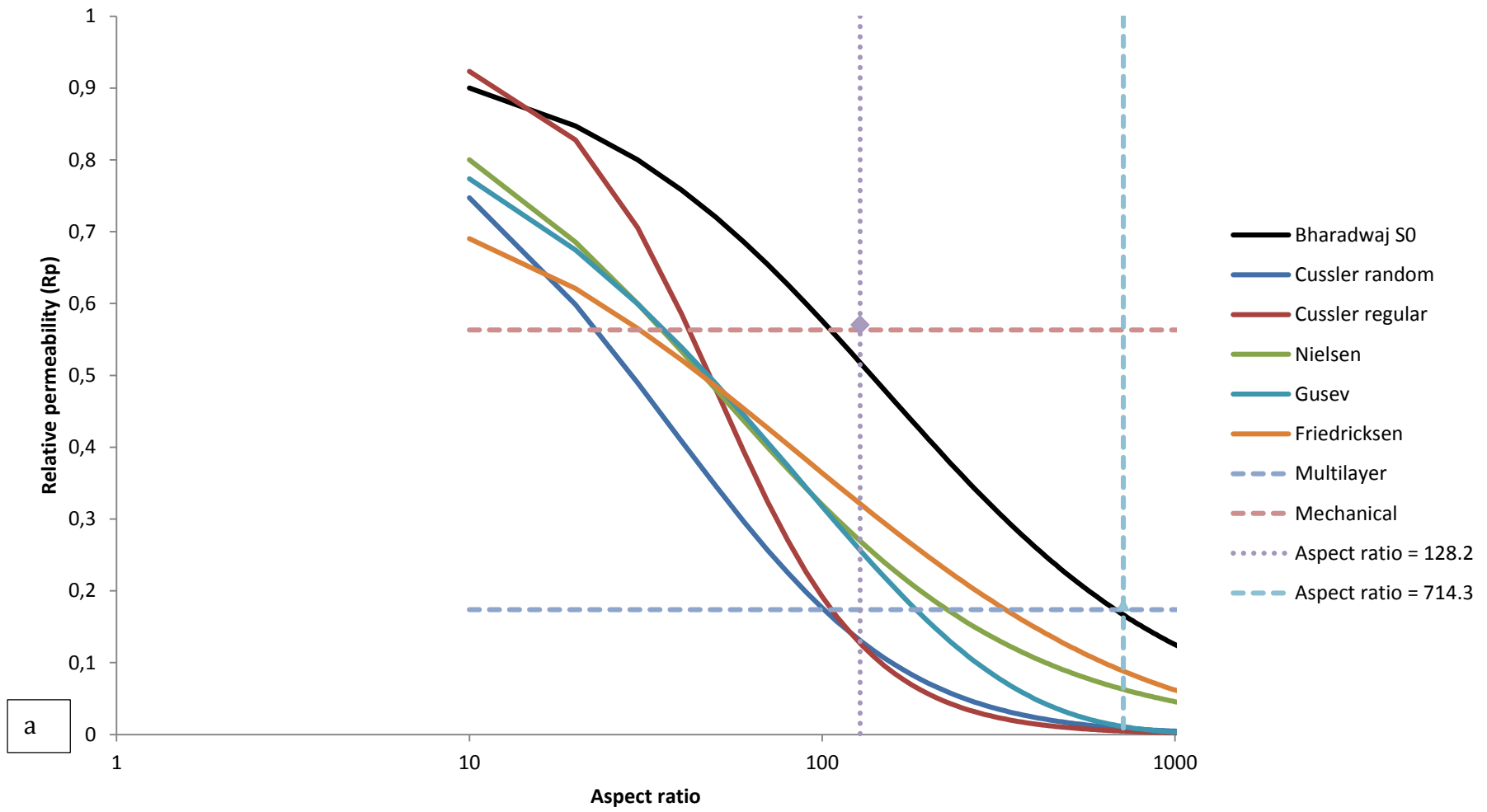
**Figure 10:** AFM image of graphene nanoplatelet demonstrating how the platelet thickness was measured.

**Table 4:** AFM measurements made of graphene nanoplatelet thickness according to the dispersion method

Measurement	Manually stirred dispersion	Ultrasonic dispersion for 30 min
1	78.683	17.070
2	104.802	11.808
3	49.608	12.534
<b>Average</b>	<b>77.7</b>	<b>13.8</b>

Using the diameter from the SEM images (10  $\mu\text{m}$ ) and the average thickness of the graphene nanoplatelets from the AFM measurements (**Table 4**), the aspect ratios were estimated as ca 128.2 for the manually stirred and ca 714.28 for the ultrasonic dispersion. The estimated aspect ratios were found to be significantly lower than the expected theoretical aspect ratio. Other researchers have also found the aspect ratio to be significantly lower when modelling the rheological properties of graphene nanoplatelets dispersed in epoxy resin [38].

To confirm these estimated aspect ratios, the relative permeabilities were plotted as a function of the aspect ratio and compared with the models for the specific loading of graphene nanoplatelets (**Fig 11**). The estimated aspect ratio of the multilayer and mechanical prepared samples (4 vol%) showed good agreement with the Bharadwaj model ( $S=0$ ) (**Fig 11a**). At a loading of 2 vol% (**Fig 11b**), the mechanical and manually dispersed samples also showed close correlation with the Bharadwaj model ( $S=0$ ). The other models assume perfect alignment parallel with the substrate surface in the polymer matrix, whereas the Bharadwaj model introduces an S-factor which compensates for orientation of the platelets. The S-value of 0 indicates a random orientation of the platelets which was observed with the microfocus x-ray tomography for the multilayer sample. In comparison with the other models, the Bharadwaj model was the most accurate at describing the aspect ratio and the helium permeability reduction of the graphene/epoxy composite samples. The model also indicates that if the orientation can be improved to where  $S = 1$ , then the relative permeability can be reduced even further.



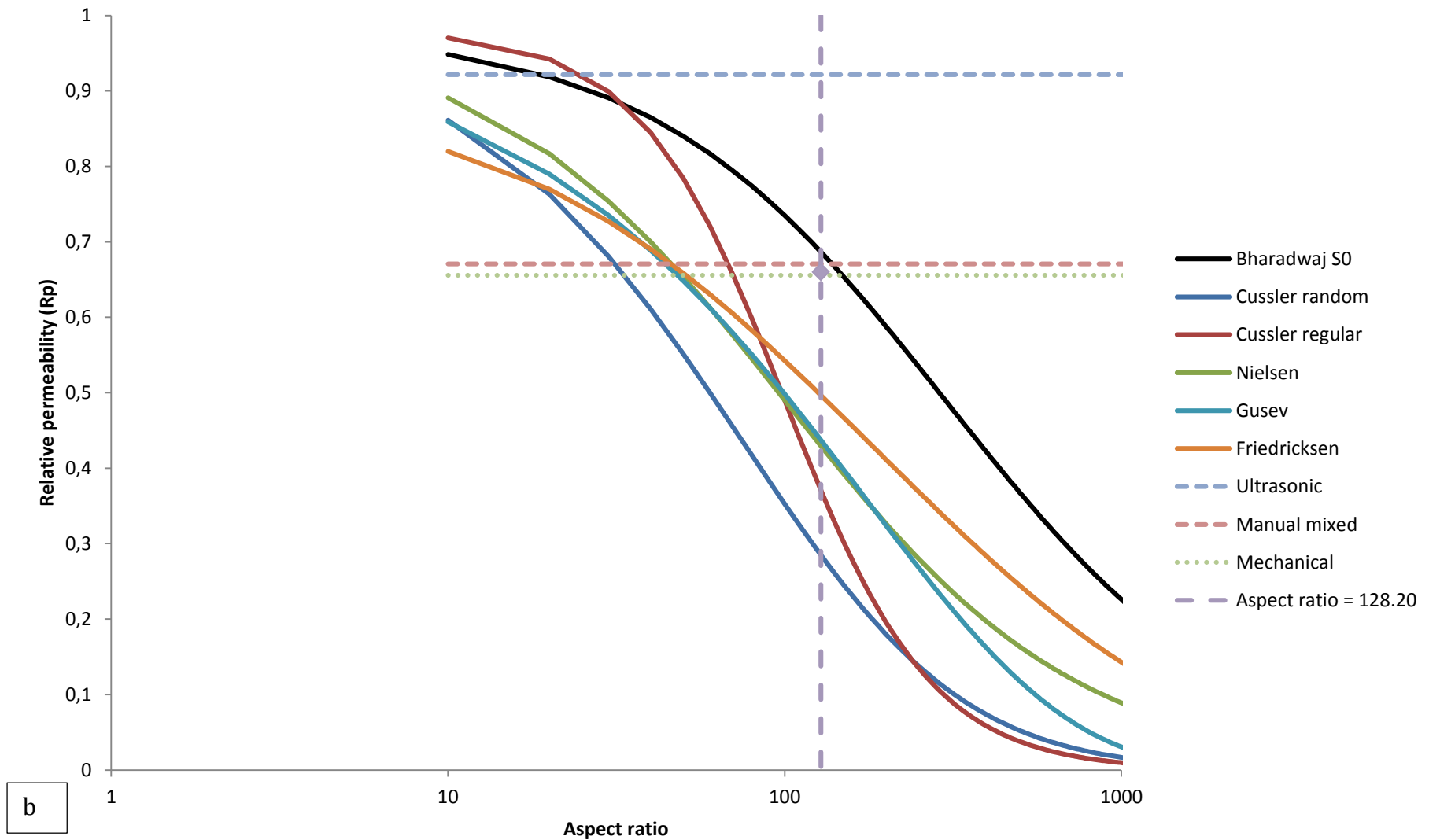


**Figure 11:** Comparison between the experimental relative permeability (Rp) and the theoretical model predictions as to verify the estimated aspect ratios for the composite samples containing (a) 4 vol% and (b) 2 vol% graphene.

## **4 Conclusion**

With this study graphene/epoxy resin composite coatings were prepared and helium gas permeation experiments were performed to evaluate if the coatings might be an effective barrier material to limit or prevent the release of tritium or other radioactive gases. The incorporation of graphene into the epoxy matrix did reduce the helium gas permeability; however, this was also dependent on how the graphene was dispersed in the polymer matrix and the sample preparation method. The techniques utilised were done so as to show how basic methods might be effective in actual practice of dispersing the graphene in an epoxy matrix and applied on a substrate surface to reduce the gas permeability. It was found that the multilayer technique combined with long sonication times reduced the helium gas permeability by 83%. The physical observations made by the characterisation methods were confirmed by modelling the gas permeability with the tortuous path theory. The Bharadwaj model was effective in confirming the calculated aspect ratio of the doctor blade sheets which were manually and mechanically dispersed and also that of the multilayer sample. Furthermore, the model accurately described the random orientation of the graphene platelets in the polymer matrix. Therefore, the graphene epoxy composite coatings might be considered as a possible method to limit the release of radioactive gases like tritium. However, confirmation studies on the long term durability will be required and how to improve the coatings even further with regards to dispersion of the graphene nanoplatelets.

## **Acknowledgements**

The authors would like to express their gratitude to Necsa for the financial support for this study. The Carbowaste/Department of Science and Technology for the funds made available to purchase the epoxy resin and the graphene nanoplatelets for the fabrication

of the composite coatings. Dr WCMH Meyer who is part of the Carbowaste project committee and initiated the project. Dr H Bisset and Mr JP le Roux (Necsa) for their valuable advice regarding the modelling of the gas permeability. Mr FC de Beer, Mr JW Hoffman, and Mr LC Bam from the Radiation Science department for the X-ray tomography performed and the DST/NRF for funding the microfocus x-ray system. Mr TP Ntsoane (Necsa) for performing the XRD analysis on the composite samples. Mr Stan Wiley from Micromeritics (USA) and Mr R van der Merwe (Necsa) for the development of a method to perform the particle size analysis on the graphene nanoplatelets. Dr J Wesley-Smith and Dr T Malwela from the CSIR for the TEM and AFM imaging of the composite samples and graphene nanoplatelets. Dr HE Oosthuizen and Mr JC Thompson for their recommendations regarding the preparation of the article.

## References

- [1] McGann OJ, Ojovan MI. The synthesis of graphite–glass composites intended for the immobilisation of waste irradiated graphite. *J Nucl Mater* 2011;413:47–52. doi:10.1016/j.jnucmat.2011.03.054.
- [2] Von Lensa W, Vulpius D, Steinmetz HJ, Girke N, Bosbach D, Thomauske B, et al. Treatment and disposal of irradiated graphite and other carbonaceous waste. *ATW-Int Z Kernenerg* 2011;56:263.
- [3] IAEA. Characterization, Treatment and Conditioning of Radioactive Graphite from Decommissioning of Nuclear Reactors 2006.
- [4] Van Rooyen LJ, Karger-Kocsis J, Vorster OC, Kock LD. Helium gas permeability reduction of epoxy composite coatings by incorporation of glass flakes. *J Membr Sci* 2013;430:203–10. doi:10.1016/j.memsci.2012.11.083.
- [5] Bushuev AV, Verzilov YM, Zubarev VN, Kachanovskii AE, Matveev OV, Proshin IM, et al. Quantitative determination of the amount of  $^3\text{H}$  and  $^{14}\text{C}$  in reactor graphite. *At Energy* 1992;73:959–62. doi:10.1007/BF00761431.
- [6] Yim M-S, Caron F. Life cycle and management of carbon-14 from nuclear power generation. *Prog Nucl Energy* 2006;48:2–36. doi:10.1016/j.pnucene.2005.04.002.
- [7] Costes JR, de Tassigny C, Vidal H. Conditioning of graphite bricks from dismantled gas-cooled reactors for disposal. *Waste Manag* 1990;10:297–302. doi:10.1016/0956-053X(90)90103-R.
- [8] Shtrombakh YI, Platonov PA, Lobanov NS, Chugunov OK, Aleksandrov VP, Zinov'ev OA. Epoxy Compounds for Immobilizing Radioactive Wastes. *At Energy* 2005;98:331–3. doi:10.1007/s10512-005-0213-7.

- [9] Amanat N, Nicoll AF, Ruys AJ, McKenzie DR, James NL. Gas permeability reduction in PEEK film: Comparison of tetrahedral amorphous carbon and titanium nanofilm coatings. *J Membr Sci* 2011;378:265–71. doi:10.1016/j.memsci.2011.05.019.
- [10] Chen J-T, Fu Y-J, An Q-F, Lo S-C, Zhong Y-Z, Hu C-C, et al. Enhancing polymer/graphene oxide gas barrier film properties by introducing new crystals. *Carbon* 2014;75:443–51. doi:10.1016/j.carbon.2014.04.024.
- [11] Qian G, Cho JW, Lan T. Nanocor | Technical Papers | Preparation and Properties of Polyolefin Nanocomposites. Tech Pap 2001. [http://www.nanocor.com/tech\\_papers/properties\\_polyolefin.asp](http://www.nanocor.com/tech_papers/properties_polyolefin.asp) (accessed January 28, 2012).
- [12] Kim H, Macosko CW. Processing-property relationships of polycarbonate/graphene composites. *Polymer* 2009;50:3797–809. doi:10.1016/j.polymer.2009.05.038.
- [13] Choudalakis G, Gotsis AD. Permeability of polymer/clay nanocomposites: A review. *Eur Polym J* 2009;45:967–84. doi:10.1016/j.eurpolymj.2009.01.027.
- [14] DeRocher JP, Gettelfinger BT, Wang J, Nuxoll EE, Cussler EL. Barrier membranes with different sizes of aligned flakes. *J Membr Sci* 2005;254:21–30. doi:10.1016/j.memsci.2004.12.025.
- [15] Dumont M-J, Reyna-Valencia A, Emond J-P, Bousmina M. Barrier properties of polypropylene/organoclay nanocomposites. *J Appl Polym Sci* 2007;103:618–25. doi:10.1002/app.25253.
- [16] Frounchi M, Dadbin S, Salehpour Z, Noferesti M. Gas barrier properties of PP/EPDM blend nanocomposites. *J Membr Sci* 2006;282:142–8. doi:10.1016/j.memsci.2006.05.016.
- [17] Kalaitzidou K, Fukushima H, Drzal LT. Multifunctional polypropylene composites produced by incorporation of exfoliated graphite nanoplatelets. *Carbon* 2007;45:1446–52. doi:10.1016/j.carbon.2007.03.029.
- [18] Kim D, Kwon H, Seo J. EVOH nanocomposite films with enhanced barrier properties under high humidity conditions. *Polym Compos* 2013;n/a – n/a. doi:10.1002/pc.22707.
- [19] Kim H, Abdala AA, Macosko CW. Graphene/Polymer Nanocomposites. *Macromolecules* 2010;43:6515–30. doi:10.1021/ma100572e.
- [20] Kim HM, Lee JK, Lee HS. Transparent and high gas barrier films based on poly(vinyl alcohol)/graphene oxide composites. *Thin Solid Films* 2011;519:7766–71. doi:10.1016/j.tsf.2011.06.016.
- [21] Kuila T, Bose S, Mishra AK, Khanra P, Kim NH, Lee JH. Effect of functionalized graphene on the physical properties of linear low density polyethylene nanocomposites. *Polym Test* 2012;31:31–8.
- [22] Lape NK, Nuxoll EE, Cussler EL. Polydisperse flakes in barrier films. *J Membr Sci* 2004;236:29–37. doi:10.1016/j.memsci.2003.12.026.
- [23] Ogasawara T, Ishida Y, Ishikawa T, Aoki T, Ogura T. Helium gas permeability of montmorillonite/epoxy nanocomposites. *Compos Part Appl Sci Manuf* 2006;37:2236–40. doi:10.1016/j.compositesa.2006.02.015.
- [24] Potts JR, Dreyer DR, Bielawski CW, Ruoff RS. Graphene-based polymer nanocomposites. *Polymer* 2011;52:5–25. doi:10.1016/j.polymer.2010.11.042.
- [25] Singh V, Joung D, Zhai L, Das S, Khondaker SI, Seal S. Graphene based materials: Past, present and future. *Prog Mater Sci* 2011;56:1178–271. doi:10.1016/j.pmatsci.2011.03.003.

- [26] Takahashi S, Goldberg HA, Feeney CA, Karim DP, Farrell M, O’Leary K, et al. Gas barrier properties of butyl rubber/vermiculite nanocomposite coatings. *Polymer* 2006;47:3083–93. doi:10.1016/j.polymer.2006.02.077.
- [27] Yao XF, Lei YM, Xiong C, Wang XQ, Wang YQ. Experimental Study on Damage-induced Helium Leakage in Flexible Composites. *J Reinf Plast Compos* 2010;29:2936–45.
- [28] Yao XF, Lei YM, Xiong C, Wang XQ, Wang YQ. Experimental study of helium leakage parameters in flexible composite. *J Appl Polym Sci* 2010;116:3562–8. doi:10.1002/app.31920.
- [29] Huang H-D, Ren P-G, Chen J, Zhang W-Q, Ji X, Li Z-M. High barrier graphene oxide nanosheet/poly(vinyl alcohol) nanocomposite films. *J Membr Sci* 2012;409–410:156–63. doi:10.1016/j.memsci.2012.03.051.
- [30] Yoo BM, Shin HJ, Yoon HW, Park HB. Graphene and graphene oxide and their uses in barrier polymers. *J Appl Polym Sci* 2014;131:39628–50. doi:10.1002/app.39628.
- [31] Berry V. Impermeability of graphene and its applications 2014.
- [32] Bunch JS, Verbridge SS, Alden JS, van der Zande AM, Parpia JM, Craighead HG, et al. Impermeable atomic membranes from graphene sheets. *Nano Lett* 2008;8:2458–62.
- [33] Nair RR, Wu HA, Jayaram PN, Grigorieva IV, Geim AK. Unimpeded permeation of water through helium-leak-tight graphene-based membranes. *Science* 2012;335:442–4.
- [34] Guo F, Silverberg G, Bowers S, Kim S-P, Datta D, Shenoy V, et al. Graphene-Based Environmental Barriers. *Environ Sci Technol* 2012;46:7717–24. doi:10.1021/es301377y.
- [35] Yang C, Smyrl WH, Cussler EL. Flake alignment in composite coatings. *J Membr Sci* 2004;231:1–12. doi:10.1016/j.memsci.2003.09.022.
- [36] Prolongo SG, Moriche R, Sánchez M, Ureña A. Self-stratifying and orientation of exfoliated few-layer graphene nanoplatelets in epoxy composites. *Compos Sci Technol* 2013;85:136–41. doi:10.1016/j.compscitech.2013.06.015.
- [37] Yasmin A, Luo J-J, Daniel IM. Processing of expanded graphite reinforced polymer nanocomposites. *Compos Sci Technol* 2006;66:1182–9. doi:10.1016/j.compscitech.2005.10.014.
- [38] Chandrasekaran S, Seidel C, Schulte K. Preparation and characterization of graphite nano-platelet (GNP)/epoxy nano-composite: Mechanical, electrical and thermal properties. *Eur Polym J* 2013;49:3878–88. doi:10.1016/j.eurpolymj.2013.10.008.
- [39] Humpenöder J. Gas permeation of fibre reinforced plastics. *Cryogenics* 1998;38:143–7. doi:10.1016/S0011-2275(97)00125-2.
- [40] Schultheiß D. Permeation Barrier for Lightweight Liquid Hydrogen Tanks. University of Augsburg, 2007.
- [41] Boukehili H, Nguyen-Tri P. Helium gas barrier and water absorption behavior of bamboo fiber reinforced recycled polypropylene. *J Reinf Plast Compos* 2012;31:1638–51. doi:10.1177/0731684412464090.
- [42] Dos Santos JMF. Simple vacuum experiments for undergraduate student laboratories. *Vacuum* 2005;80:258–63. doi:10.1016/j.vacuum.2005.07.043.
- [43] Maji PK, Das NK, Bhowmick AK. Preparation and properties of polyurethane nanocomposites of novel architecture as advanced barrier materials. *Polymer* 2010;51:1100–10. doi:10.1016/j.polymer.2009.12.040.

- [44] Muller K, Botos J, Bastian M, Heidemeyer P, Hochrein T. Faster Results. *Kunststoffe Int* 2011;62-7.
- [45] Yokozeki T, Aoki T, Ishikawa T. The effect of matrix cracks on gas permeability through CFRP laminates. *Adv Compos Mater* 2004;13:227-36. doi:10.1163/1568551042580136.
- [46] J. Hoffman, F. De Beer. Characteristics of the Micro-Focus X-ray Tomography System at the MIXRAD Facility at NECSA in South Africa, Durban, South Africa: <http://www.ndt.net/>; 2012.
- [47] Chong HM, Taylor AC. The Effect of Graphene Nanoplatelets on the Fracture Toughness of Epoxy Polymers 2014.
- [48] Rogers WA, Buritz RS, Alpert D. Diffusion Coefficient, Solubility, and Permeability for Helium in Glass. *J Appl Phys* 1954;25:868-75.
- [49] Kosmidou TV. Structural, mechanical and electrical characterization of epoxy-amine/carbon black nanocomposites. *EXPRESS Polym Lett* 2008;2:364-72. doi:10.3144/expresspolymlett.2008.43.
- [50] Bhattacharya M, Biswas S, Bhowmick AK. Permeation characteristics and modeling of barrier properties of multifunctional rubber nanocomposites. *Polymer* 2011;52:1562-76. doi:10.1016/j.polymer.2011.01.055.
- [51] Gatos KG, Karger-Kocsis J. Effect of the aspect ratio of silicate platelets on the mechanical and barrier properties of hydrogenated acrylonitrile butadiene rubber (HNBR)/layered silicate nanocomposites. *Eur Polym J* 2007;43:1097-104. doi:10.1016/j.eurpolymj.2007.01.032.
- [52] Picard E, Vermogen A, Gérard J-F, Espuche E. Barrier properties of nylon 6-montmorillonite nanocomposite membranes prepared by melt blending: Influence of the clay content and dispersion state: Consequences on modelling. *J Membr Sci* 2007;292:133-44. doi:10.1016/j.memsci.2007.01.030.
- [53] Sun L, Boo W-J, Clearfield A, Sue H-J, Pham HQ. Barrier properties of model epoxy nanocomposites. *J Membr Sci* 2008;318:129-36. doi:10.1016/j.memsci.2008.02.041.
- [54] Bharadwaj RK. Modeling the Barrier Properties of Polymer-Layered Silicate Nanocomposites. *Macromolecules* 2001;34:9189-92. doi:10.1021/ma010780b.
- [55] Fredrickson GH, Bicerano J. Barrier properties of oriented disk composites. *J Chem Phys* 1999;110:2181-8. doi:doi:10.1063/1.477829.
- [56] Gusev AA, Lusti HR. Rational Design of Nanocomposites for Barrier Applications. *Adv Mater* 2001;13:1641-3. doi:10.1002/1521-4095(200111)13:21<1641::AID-ADMA1641>3.0.CO;2-P.
- [57] Nielsen LE. Models for the Permeability of Filled Polymer Systems. *J Macromol Sci Part - Chem* 1967;1:929-42. doi:10.1080/10601326708053745.